

Two-Dimensional Layered Heterostructures Synthesized from Core–Shell Nanowires**

Qi Zhang, Xu Xiao, Ruiqi Zhao, Danhui Lv, Guanchen Xu, Zhixing Lu, Lifei Sun, Shizhe Lin, Xiang Gao, Jun Zhou, Chuanhong Jin, Feng Ding, and Liying Jiao*

Abstract: Controlled stacking of different two-dimensional (2D) atomic layers will greatly expand the family of 2D materials and broaden their applications. A novel approach for synthesizing MoS_2/WS_2 heterostructures by chemical vapor deposition has been developed. The successful synthesis of pristine MoS_2/WS_2 heterostructures is attributed to using core-shell $\text{WO}_{3-x}/\text{MoO}_{3-x}$ nanowires as a precursor, which naturally ensures the sequential growth of MoS_2 and WS_2 . The obtained heterostructures exhibited high crystallinity, strong interlayer interaction, and high mobility, suggesting their promising applications in nanoelectronics. The stacking orientations of the two layers were also explored from both experimental and theoretical aspects. It is elucidated that the rational design of precursors can accurately control the growth of high-quality 2D heterostructures. Moreover, this simple approach opens up a new way for creating various novel 2D heterostructures by using a large variety of heteronanomaterials as precursors.

Two-dimensional (2D) atomic crystals have emerged as promising building blocks for functional architectures and devices owing to their unique planar structure and distinct electrical and optical properties.^[1] The vertical stacking of graphene and hexagonal boron nitride (h-BN) provides a unique platform for exploring new phenomenon in condensed matter physics and has been successfully demonstrated in fabricating field-effect tunneling transistors.^[1c,2] Compared with graphene and h-BN, the 2D transition-metal dichalcogenides (TMDCs) are more promising for building layered heterostructures owing to their diverse compositions and electronic structures.^[3] Recently, the 2D MoS_2/WS_2 semiconducting heterostructures have been achieved by

sequentially transferring MoS_2 and WS_2 single layers and ultrafast charge transfer has been observed in the heterostructure, suggesting its potential application in optoelectronics.^[4] However, the stacking of 2D materials by transfer may introduce impurities and/or strain to the interface between the two layers and thus degrade the layer–layer interactions. Therefore, achieving the stacking of different TMDCs layers in a controllable manner by direct CVD growth is highly desirable. Experimentally, it is a great challenge to synthesize the MoS_2/WS_2 bilayers owing to the preferred formation of $\text{Mo}_x\text{W}_{1-x}\text{S}_2$ alloys, which is driven by the high configuration entropy.^[5] Very recently the direct growth of MoS_2/WS_2 heterostructures has been attempted by two individual groups. Cao et al. utilized the mixture of MoO_3 and WO_3 as precursors and obtained alloyed WS_2/MoS_2 bilayers with about 5–10% of the other component in each layer,^[6] further indicating the difficulties in producing pristine MoS_2/WS_2 heterostructure. Ajayan and co-workers reported the successful growth of vertical and in-plane heterostructures of MoS_2/WS_2 through tellurium-mediated sulfurization of MoO_3 and W.^[7] However, the Te mediator introduced several intermediate products and thus made the chemical reactions very complicated. Thus far, a simple and well-controlled chemical approach that allows the sequential growth of high quality MoS_2 and WS_2 to form the MoS_2/WS_2 heterostructures is still lacking.

The major challenge in the growth of MoS_2/WS_2 heterostructures is the sequential feeding of Mo and W to avoid the formation of the alloys. To address this challenge, we designed a synthesis strategy for growing pure MoS_2/WS_2 2D heterostructures by the gas phase sulfurization of core–shell nano-

[*] Q. Zhang,^[‡] G. Xu, Z. Lu, L. Sun, Prof. L. Jiao
Key Laboratory of Organic Optoelectronics and
Molecular Engineering of the Ministry of Education
Department of Chemistry
Tsinghua University, Beijing 100084 (China)
E-mail: lyjiao@mail.tsinghua.edu.cn

X. Xiao,^[‡] S. Lin, X. Gao, Prof. J. Zhou
School of Optical and Electronic Information
Huazhong University of Science and Technology
Wuhan 430074 (China)


Dr. R. Zhao
College of Physics and Chemistry
Henan Polytechnic University
Henan 454033 (China)

D. Lv, Prof. C. Jin
State Key Laboratory of Silicon Materials
School of Materials Science & Engineering
Zhejiang University, Hangzhou, Zhejiang 310027 (China)

Prof. F. Ding
Institute of Textile and Clothing
Hong Kong Polytechnic University, Kowloon, Hong Kong (China)

[‡] These authors contributed equally to this work.

[**] L.J. acknowledges NSFC (21322303, 51372134), National Program for Thousand Young Talents of China, Tsinghua University Initiative Scientific Research Program, and Tsinghua-Foxconn Nanotechnology Research Center Research Program. R.Z. acknowledges NSFC (21303041), Beijing National Laboratory for Molecular Sciences (2013006), and high-performance grid computing platform of Henan Polytechnic University. J.Z. acknowledges NSFC (51322210, 61434001) and Director Fund of WNLO. C.J. acknowledges NSFC (51222202, 51410305074 and 51472215), the MOST (2014CB932500 and 2015CB921000), and the Fundamental Research Funds for the Central Universities (2014XZZX003-07).

 Supporting information for this article is available on the WWW under <http://dx.doi.org/10.1002/anie.201502461>.

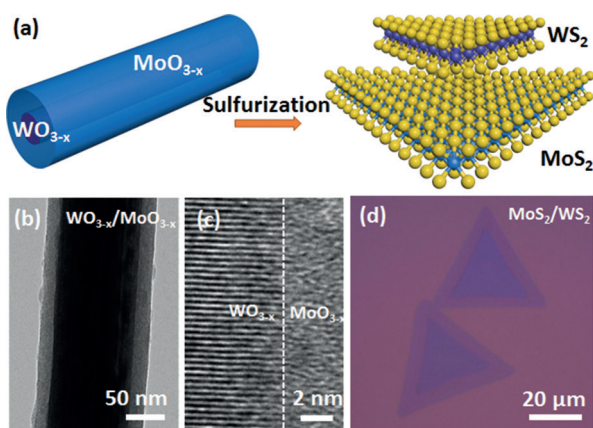


Figure 1. Synthesis of MoS_2/WS_2 heterostructures using $\text{WO}_{3-x}/\text{MoO}_{3-x}$ core-shell nanowires as precursor. a) Representation of the synthesis of the MoS_2/WS_2 bilayer. b) Typical TEM image of a $\text{WO}_{3-x}/\text{MoO}_{3-x}$ core-shell nanowire with a core diameter of about 100 nm and shell thickness of about 20 nm. c) High-resolution TEM image of the interface of WO_{3-x} and MoO_{3-x} , showing high crystallinity of the WO_{3-x} . d) Optical image of the typical MoS_2/WS_2 bilayer flakes after the CVD growth.

wires with WO_{3-x} as the core and MoO_{3-x} as the shell. The core-shell structure together with the significantly higher sublimation temperature of WO_{3-x} than that of MoO_{3-x} naturally ensures the sequential sublimation of MoO_{3-x} and WO_{3-x} at a suitable temperature and thus results in the sequent growth of MoS_2 and WS_2 (Figure 1 a).

The chemical reactions involved in this growth are simply the gas-phase sulfurization of MoO_{3-x} and WO_{3-x} , both of which are well-known.^[8] The core-shell $\text{WO}_{3-x}/\text{MoO}_{3-x}$ nanowires were prepared by using the CVD-grown single crystalline WO_{3-x} nanowires as the template for the electrochemical deposition of amorphous MoO_{3-x} (see experimental details in Supporting Information).^[9] The different crystalline quality enlarges the difference of sublimation temperature between the two oxides, further avoiding the mixing of the two oxides. A transmission electron microscope (TEM) image clearly demonstrates the core-shell structure of a $\text{WO}_{3-x}/\text{MoO}_{3-x}$ nanowire with a diameter of about 140 nm (Figure 1 b). A higher-resolution TEM image taken at the interface of $\text{WO}_{3-x}/\text{MoO}_{3-x}$ reveals the highly crystalline WO_{3-x} and amorphous MoO_{3-x} in the nanowire (Figure 1 c). The CVD growth of MoS_2/WS_2 bilayers was carried out in a CVD furnace by gas-phase sulfurization of $\text{WO}_{3-x}/\text{MoO}_{3-x}$ nanowires in sulfur vapor carried by Ar flow at about 780–850 °C (Supporting Information, Figures S1 and S2). After the growth, triangular bilayered flakes with edge length of about 20–40 μm were resolved under optical microscope (Figure 1 d). In-plane MoS_2/WS_2 monolayers and $\text{Mo}_x\text{W}_{1-x}\text{S}_2$ alloys were obtained at temperatures higher than 850 °C (Supporting Information, Figures S3 and S4).

Micro-Raman spectroscopy was utilized to characterize the composition of the MoS_2/WS_2 heterostructures. Raman intensity mapping image of the MoS_2/WS_2 bilayer shown in Figure 2 a with 404 cm^{-1} (A_{1g} mode of MoS_2 , blue) and 417 cm^{-1} (A_{1g} mode of WS_2 , red) clearly displays the vertical stacking of the two layers (Figure 2 b). The Raman spectra

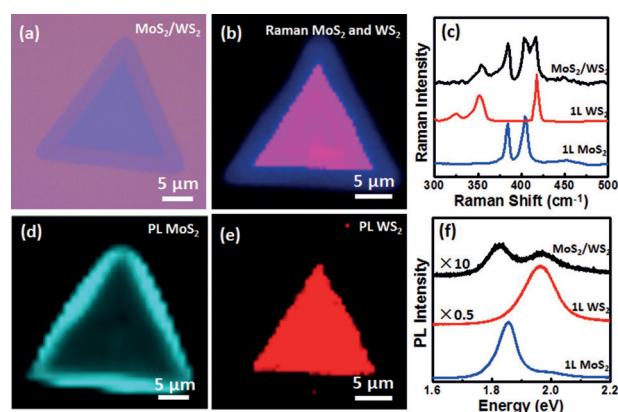


Figure 2. Raman and PL characterizations of the MoS_2/WS_2 heterostructures. a) Optical image of a MoS_2/WS_2 bilayer flake with a lateral size of about 25 μm. b) Raman mapping image of the flake shown in (a) with 404 cm^{-1} (A_{1g} mode of MoS_2 , blue) and 417 cm^{-1} (A_{1g} mode of WS_2 , red) peak intensities using 514 nm laser excitation. c) and f) Typical Raman and PL spectra of single-layer MoS_2 , WS_2 , and MoS_2/WS_2 bilayers, respectively. d) and e) PL mapping image of the same flake with 1.84 eV (A-exciton peak of MoS_2) and 1.97 eV (A-exciton peak of WS_2), respectively.

taken on the bilayer region show 4 discrete peaks, which precisely correspond to the E_{2g}^1 and A_{1g} modes of single layer MoS_2 and WS_2 (Figure 2 c; Supporting Information, Figure S5b). This is distinctly different from the Raman spectra of $\text{Mo}_x\text{W}_{1-x}\text{S}_2$ alloy, which shows only two prominent peaks^[10] (Supporting Information, Figure S7). Therefore, we can distinguish the MoS_2/WS_2 vertical stacking layers from the alloy easily using Raman spectroscopy. AFM image taken on the same MoS_2/WS_2 bilayer flake shows that the thickness of each layer is about 0.7 nm (Supporting Information, Figure S5e,f), which reveals the single-layer nature of both layers.

Photoluminescence (PL) spectroscopy is used to study the interlayer interaction in the MoS_2/WS_2 heterostructure. PL mapping images of the MoS_2/WS_2 bilayer were taken with the A-exciton resonances of MoS_2 (ca. 1.84 eV, Figure 2 d) and WS_2 (ca. 1.97 eV, Figure 2 e), respectively. The PL intensity map shown in Figure 2 d clearly demonstrates that the PL signals from the bilayered region are significantly lower than those from the single layer MoS_2 . The drastic quenching of PL signals from the heterostructures was further confirmed by comparing the typical PL spectra of MoS_2/WS_2 bilayers with those of single layer MoS_2 and WS_2 (Figure 2 f). The intensities of the A-exciton peaks of MoS_2 and WS_2 in the bilayer region are about 20 and about 80 times lower than that of the single layer MoS_2 and WS_2 , respectively. The dramatic quenching of PL in the heterostructures is in consistent with previous optical studies on transferred and CVD-grown MoS_2/WS_2 bilayers and was attributed to the strong interlayer interaction and efficient charge transfer in the type II heterostructures.^[4a,6] In contrast to the great change in peak intensity, the positions of PL peaks of MoS_2 and WS_2 did not shift much in the heterostructure region, which is in accordance with the theoretical prediction that the K -point of the band structures of the heterostructure may not change obviously.^[11] Similar to recent reports on PL of MoS_2/WS_2

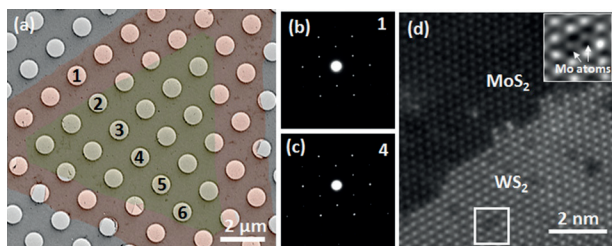


Figure 3. TEM characterizations of the MoS₂/WS₂ heterostructures. a) TEM image of a MoS₂/WS₂ bilayer flake supported on a holey carbon TEM grid. To increase the contrast between the supporting film and the bilayers, the color of MoS₂ and WS₂ was rendered to light red and green, respectively. b) and c) SAED patterns taken at locations marked with 1 and 4 on the MoS₂/WS₂ bilayer flake in (a). The SAED patterns of 2, 3, 5, and 6 are shown in the Supporting Information, Figure S6. d) Atomic-resolution STEM image of a MoS₂/WS₂ step edge with a roughness of a few atoms (Note: this image was not taken on the flake shown in (a)). Inset: fast Fourier transform (FFT) filtered image of the area marked with the white box, showing the substitution of W atoms with Mo atoms.

heterostructures,^[4a,6] the PL peak at 1.4 eV which was detected in the MoS₂/WS₂ bilayers synthesized with the aid of Te^[7] was also not observed in our samples.

We then conducted TEM and selected-area electron diffraction (SAED) studies to evaluate the crystallinity of the MoS₂/WS₂ heterostructures by transferring the as-grown samples to holey carbon TEM grids.^[12] Figure 3a displays the TEM image of a MoS₂/WS₂ bilayer with a lateral size of about 12 and about 20 μm , respectively. The collected SAED patterns at multiple locations of the MoS₂/WS₂ bilayer were shown in Figure 3b,c and the Supporting Information, Figure S6. All the patterns we acquired display a hexagonal symmetry of 2H-MoS₂ or WS₂ with the same spatial arrangement and orientation, indicating the single crystalline nature of the CVD-grown MoS₂/WS₂ heterostructure over a very large area. Here, only one set of SAED pattern was observed on the MoS₂/WS₂ bilayer owing to the same lattice orientation in the two layers (twisted angle $\theta = 0^\circ$) and the almost identical lattice constants of MoS₂ (3.160 Å) and WS₂ (3.153 Å).^[13] We also characterized the step edges of the MoS₂/WS₂ heterostructures with scanning transmission electron microscopy (STEM). The distribution of Mo and W atoms can be easily identified by their obviously different annular dark-field (ADF) contrast owing to their different Z values in the atomic resolution STEM image (Figure 3d).^[10] Very few W atoms were resolved in the bottom MoS₂ layer (<0.5%) and less than 3% W atoms were substituted by Mo atoms in the top WS₂ layer, indicating a higher purity of the heterostructures than those made by previous methods.^[6,7]

Although the bilayer MoS₂/WS₂ heterostructures with the same orientation were found to dominate the heterostructure products with a relatively large top layer (the length ratio between the two layers $a/b > 0.3$), those with opposite orientation ($\theta = 60^\circ$) were also frequently observed for products with smaller top layer ($a/b < 0.3$), and, occasionally, those with twist angles of about $20 \pm 2^\circ$ were also found (Figure 4a; Supporting Information, Figure S8). We performed van der Waals corrected density functional theory (VDW-DFT) calculations to explore the relative stability of

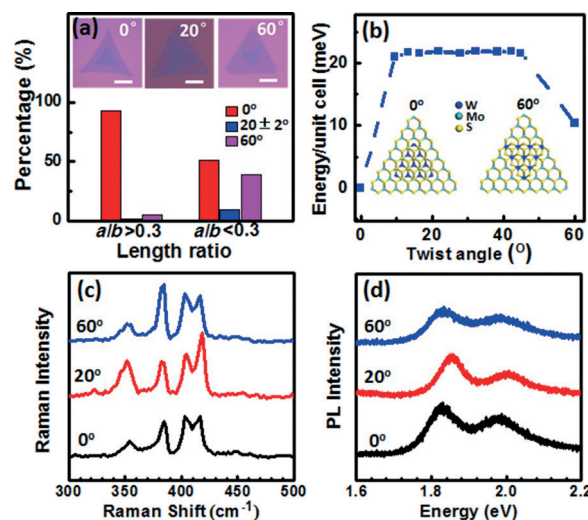


Figure 4. Stacking orientations in the MoS₂/WS₂ heterostructures. a) Distribution of twist angles in about 200 MoS₂/WS₂ bilayers. Insets: optical images of the CVD-grown MoS₂/WS₂ bilayer flakes with twist angles of 0° , 20° , and 60° . Scale bar: 10 μm . b) Relative formation energies of MoS₂/WS₂ as a function of the twist angles by VDW-DFT calculations. Insets: representations of MoS₂/WS₂ bilayers with twist angles of 0° and 60° . c) and d) Typical Raman and PL spectra of MoS₂/WS₂ bilayers with twist angles of 0° , 20° , and 60° , respectively.

MoS₂/WS₂ bilayers with different stacking orientations (see calculation details in Supporting Information and Figure S9). The theoretical results shown in Figure 4b indicate that $\theta = 0^\circ$ is the global minimum of the energy surface and $\theta = 60^\circ$ is a local minimum with about 10 meV/unit cell higher energy than $\theta = 0^\circ$. All other heterostructures are less stable, which is due to the even higher and almost constant formation energy. This theoretical result is in good agreement with the uneven distribution of twist angles in the heterostructures. As the calculated energy differences among various heterostructures are small (ca. 10–20 meV/unit cell), the appearance of heterostructures with medium orientation angle (ca. $20 \pm 2^\circ$) should not be totally forbidden. And the dominating heterostructures that with $\theta = 0^\circ$ and larger top layer may be attributed to kinetics of heterostructures growth that the top layer with $\theta = 0^\circ$ grows faster than the top layers with other orientations.

Stacking configurations can dramatically tune the band structures of bilayer graphene and MoS₂.^[14] However, the stacking orientations of the two layers may not significantly affect the bandgap of the MoS₂/WS₂ heterostructures as suggested by recent theoretical calculations.^[4b,c] To verify this prediction, we studied the stacking-orientation-dependent Raman and PL spectroscopy. There are no observable shifts ($< 1 \text{ cm}^{-1}$) in the Raman spectra of MoS₂/WS₂ heterostructures with $\theta = 0^\circ$, 20° , and 60° , respectively (Figure 4c). The peak positions of A-exciton for both MoS₂ and WS₂ are almost the same for bilayers with $\theta = 0^\circ$ and 60° , respectively, but both peaks are upshifted by about 0 meV in $\theta = 20^\circ$ heterostructures (Figure 4d). These results reveal that stacking orientations of the two layers does modify the bandstructure of heterostructures, but the amplitude is negligible.

To investigate the electrical performance of the MoS₂/WS₂ heterostructures, we fabricated back-gated field effect tran-

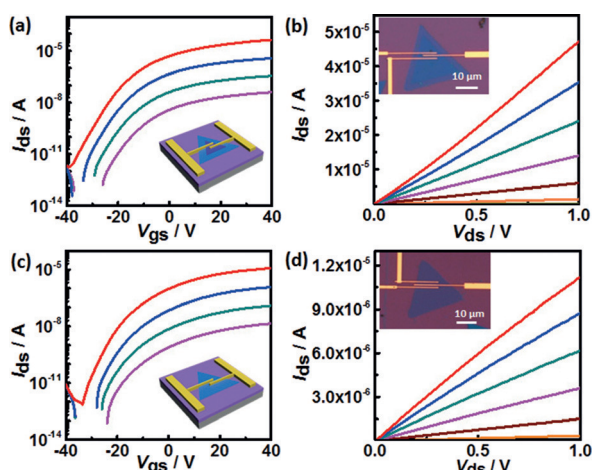


Figure 5. Electrical properties of the MoS₂/WS₂ bilayers and MoS₂ single layers. a) and c) I_{ds} - V_{gs} curves of a MoS₂/WS₂ bilayer flake (inset of b) and a single-layer MoS₂ flake (inset of d) measured at various bias voltages, respectively. The bias voltage for each curve is 1 V, 100 mV, 10 mV, and 1 mV from top to bottom. Insets of (a) and (c): representations of the back-gated FETs with MoS₂/WS₂ and single layer MoS₂ as channels, respectively. b) and d) I_{ds} - V_{ds} curves for the device in (a) and (c) at varied V_{gs} from -40 V to 40 V at a step of 10 V from bottom to top, respectively. Insets: optical images of the measured devices.

sistors (FETs) by electron beam lithography (EBL) and electron beam deposition. The transfer characteristics of a MoS₂/WS₂ bilayer measured at room temperature in vacuum (ca. 10^{-6} mbar) behaves as an n-type semiconductor with an on/off current ratio of about 10^7 (Figure 5a and b) and the estimated mobility of this device is about $30\text{ cm}^2\text{ V}^{-1}\text{ s}^{-1}$. The mobility is about five times higher than the FET made on single-layer MoS₂ (Figure 5c and d), comparable to the MoS₂/WS₂ bilayers grown with Te,^[7] and much higher than bilayer MoS₂ made by mechanical exfoliation or CVD growth (ca. $0.1\text{--}17\text{ cm}^2\text{ V}^{-1}\text{ s}^{-1}$)^[15] and MoS₂/WS₂ bilayers made by sequential transfer ($<1\text{ cm}^2\text{ V}^{-1}\text{ s}^{-1}$)^[7] with a similar device configuration. The high on/off current ratio and mobility of the MoS₂/WS₂ bilayers further demonstrated the high crystallinity of each layer in the heterostructures and clean interface between the layers.

In summary, we demonstrated the successful growth of high quality 2D MoS₂/WS₂ heterostructures by using core-shell WO_{3-x}/MoO_{3-x} nanowires as a precursor in a CVD process. The core-shell structure of the oxide precursors allowed for the sequential feeding of MoO_{3-x} and WO_{3-x} to ensure the growth of MoS₂ and WS₂ layer by layer. We also explored the selectivity and effects of the stacking orientation in the heterostructures and concluded that the difference in the bandgap of MoS₂/WS₂ bilayers introduced by varied stacking configurations was very small. This synthesis strategy can be extended to create versatile 2D TMDCs heterostructures by using various core-shell nanomaterials^[16] as precursors, and therefore will open up a new way to expand the family of 2D atomic crystals.

Keywords: chemical vapor deposition · core-shell nanowires · heterostructures · molybdenum sulfide · tungsten sulfide

How to cite: *Angew. Chem. Int. Ed.* **2015**, *54*, 8957–8960
Angew. Chem. **2015**, *127*, 9085–9088

- a) C. R. Dean, A. F. Young, I. Meric, C. Lee, L. Wang, S. Sorgenfrei, K. Watanabe, T. Taniguchi, P. Kim, K. L. Shepard, J. Hone, *Nat. Nanotechnol.* **2010**, *5*, 722–726; b) A. K. Geim, I. V. Grigorieva, *Nature* **2013**, *499*, 419–425; c) T. Georgiou, R. Jalil, B. D. Belle, L. Britnell, R. V. Gorbachev, S. V. Morozov, Y. J. Kim, A. Gholinia, S. J. Haigh, O. Makarovskiy, L. Eaves, L. A. Ponomarenko, A. K. Geim, K. S. Novoselov, A. Mishchenko, *Nat. Nanotechnol.* **2013**, *8*, 100–103; d) L. Ju, J. Velasco Jr, E. Huang, S. Kahn, C. Nisiglia, H. Tsai, W. Yang, T. Taniguchi, K. Watanabe, Y. Zhang, G. Zhang, M. Crommie, A. Zettl, F. Wang, *Nat. Nanotechnol.* **2014**, *9*, 348–352.
- L. Britnell, R. V. Gorbachev, R. Jalil, B. D. Belle, F. Schedin, A. Mishchenko, T. Georgiou, M. I. Katsnelson, L. Eaves, S. V. Morozov, N. M. R. Peres, J. Leist, A. K. Geim, K. S. Novoselov, L. A. Ponomarenko, *Science* **2012**, *335*, 947–950.
- X. Huang, Z. Zeng, H. Zhang, *Chem. Soc. Rev.* **2013**, *42*, 1934–1946.
- a) X. Hong, J. Kim, S. Shi, Y. Zhang, C. Jin, Y. Sun, S. Tongay, J. Wu, Y. Zhang, F. Wang, *Nat. Nanotechnol.* **2014**, *9*, 682–686; b) S. Tongay, W. Fan, J. Kang, J. Park, U. Koldemir, J. Suh, D. S. Narang, K. Liu, J. Ji, J. Li, R. Sinclair, J. Wu, *Nano Lett.* **2014**, *14*, 3185–3190; c) J. Yuan, S. Najmaei, Z. Zhang, J. Zhang, S. Lei, P. M. Ajayan, B. I. Yakobson, J. Lou, *ACS Nano* **2015**, *9*, 555–563.
- H. P. Komsa, A. V. Krasheninnikov, *J. Phys. Chem. Lett.* **2012**, *3*, 3652–3656.
- Y. Yu, S. Hu, L. Su, L. Huang, Y. Liu, Z. Jin, A. A. Purezky, D. B. Geohegan, K. W. Kim, Y. Zhang, L. Cao, *Nano Lett.* **2015**, *15*, 486–491.
- Y. Gong, J. Lin, X. Wang, G. Shi, S. Lei, Z. Lin, X. Zou, G. Ye, R. Vajtai, B. I. Yakobson, H. Terrones, M. Terrones, B. K. Tay, J. Lou, S. T. Pantelides, Z. Liu, W. Zhou, P. M. Ajayan, *Nat. Mater.* **2014**, *13*, 1135–1142.
- a) H. R. Gutiérrez, N. Perea-López, A. L. Elías, A. Berkdemir, B. Wang, R. Lv, F. López-Urías, V. H. Crespi, H. Terrones, M. Terrones, *Nano Lett.* **2013**, *13*, 3447–3454; b) S. Najmaei, Z. Liu, W. Zhou, X. Zou, G. Shi, S. Lei, B. I. Yakobson, J. C. Idrobo, P. M. Ajayan, J. Lou, *Nat. Mater.* **2013**, *12*, 754–759.
- X. Xiao, T. Ding, L. Yuan, Y. Shen, Q. Zhong, X. Zhang, Y. Cao, B. Hu, T. Zhai, L. Gong, J. Chen, Y. Tong, J. Zhou, Z. Wang, *Adv. Energy Mater.* **2012**, *2*, 1328–1332.
- Y. Chen, J. Xi, D. O. Dumcenco, Z. Liu, K. Suenaga, D. Wang, Z. Shuai, Y. Huang, L. Xie, *ACS Nano* **2013**, *7*, 4610–4616.
- K. Kośmider, J. Fernández-Rossier, *Phys. Rev. B* **2013**, *87*, 075451.
- L. Jiao, B. Fan, X. Xian, Z. Wu, J. Zhang, Z. Liu, *J. Am. Chem. Soc.* **2008**, *130*, 12612–12613.
- J. Xi, T. Zhao, D. Wang, Z. Shuai, *J. Phys. Chem. Lett.* **2014**, *5*, 285–291.
- a) A. Luican, G. H. Li, A. Reina, J. Kong, R. R. Nair, K. S. Novoselov, A. K. Geim, E. Y. Andrei, *Phys. Rev. Lett.* **2011**, *106*, 126802; b) K. Liu, L. Zhang, T. Cao, C. Jin, D. Qiu, Q. Zhou, A. Zettl, P. Yang, S. G. Louie, F. Wang, *Nat. Commun.* **2014**, *5*, 4966.
- a) X. Wang, H. Feng, Y. Wu, L. Jiao, *J. Am. Chem. Soc.* **2013**, *135*, 5304–5307; b) W. Wu, D. De, S. Chang, Y. Wang, H. Peng, J. Bao, S. Pei, *Appl. Phys. Lett.* **2013**, *102*, 142106.
- a) S. E. Habas, H. Lee, V. Radmilovic, G. A. Somorjai, P. Yang, *Nat. Mater.* **2007**, *6*, 692–697; b) R. Ghosh Chaudhuri, S. Paria, *Chem. Rev.* **2012**, *112*, 2373–2433.

Received: March 16, 2015

Published online: June 26, 2015